Measurement of Jet Shapes in $\bar{p}p$ Collisions at $\sqrt{s} = 1.8$ TeV

F. Abe,[11] D. Amidei,[14] C. Anway-Weiss,[3] G. Apollinari,[20] M. Atac,[6] P. Auchincloss,[19] A. R. Baden,[8] N. Bacchetta,[15] W. Badgett,[14] M. W. Bailey,[18] A. Bamberger,[6],(a) P. de Barbaro,[19] A. Barbaro-Galtieri,[12] V. E. Barnes,[18] B. A. Barnett,[10] G. Bauer,[13] T. Baumann,[8] F. Bedeschi,[17] S. Behrends,[2] S. Belforte,[17] G. Bellettini,[17] J. Bellinger,[25] D. Benjamin,[24] J. Benlloch,[6],(a) J. Bensinger,[2] A. Beretvas,[6] J. P. Berge,[6] S. Bertolucci,[7] S. Bhadra,[9] M. Binkley,[6] D. Bisello,[15] R. Blair,[1] C. Blocker,[2] A. Bodek,[19] V. Bolognesi,[17] A. W. Booth,[6] C. Boswell,[10] G. Brandenburg,[8] D. Brown,[8] E. Buckley-Geer,[21] H. S. Budd,[19] G. Busetto,[15] A. Byon-Wagner,[6] K. L. Byrum,[25] C. Campagnari,[6] M. Campbell,[14] A. Caner,[6] R. Carey,[8] W. Carithers,[12] D. Carlsmith,[25] J. T. Carroll,[6] R. Cashmore,[6],(a) A. Castro,[15] F. Cervelli,[17] K. Chadwick,[6] J. Chapman,[14] G. Chiarelli,[7] W. Chinowsky,[12] S. Cihangir,[6] A. G. Clark,[6] M. Cobal,[17] D. Connor,[16] M. Contreras,[4] J. Cooper,[6] M. Cordelli,[7] D. Crane,[6] J. D. Cunningham,[2] C. Day,[6] F. DeJongh,[6] S. Dell'Agnello,[17] M. Dell'Orso,[17] L. Demortier,[2] B. Denby,[6] P. F. Derwent,[14] T. Devlin,[21] D. DiBitonto,[22] M. Dickson,[20] R. B. Drucker,[12] K. Einsweiler,[12] J. E. Elias,[6] R. Ely,[12] S. Eno,[4] S. Errede,[9] A. Etchegoyen,[6],(a) B. Farhat,[13] B. Flaugher,[6] G. W. Foster,[6] M. Franklin,[8] J. Freeman,[6] H. Frisch,[4] T. Fuess,[6] Y. Fukui,[11] A. F. Garfinkel,[18] A. Gauthier,[9] S. Geer,[6] D. W. Gerdes,[4] P. Giannetti,[17] N. Giokaris,[20] P. Giromini,[7] L. Gladney,[16] M. Gold,[12] K. Goulianos,[20] H. Grassmann,[15] G. M. Grieco,[17] C. Grosso-Pilcher,[4] C. Haber,[12] S. R. Hahn,[6] R. Handler,[25] K. Hara,[23] B. Harral,[16] R. M. Harris,[6] S. A. Hauger,[5] J. Hauser,[3] C. Hawk,[21] T. Hessing,[22] R. Hollebeek,[16] L. Holloway,[9] S. Hong,[14] P. Hu,[21] B. Hubbard,[12] B. T. Huffman,[18] R. Hughes,[16] P. Hurst,[8] J. Huth,[6] J. Hylen,[6] M. Incagli,[17] T. Ino,[23] H. Iso,[23] H. Jensen,[6] C. P. Jessop,[8] R. P. Johnson,[6] U. Joshi,[6] R. W. Kadel,[12] T. Kamon,[22] S. Kanda,[23] D. A. Kardelis,[9] I. Karliner,[9] E. Kearns,[8] L. Keeble,[22] R. Kephart,[6] P. Kesten,[2] R. M. Keup,[9] H. Keutelian,[6] D. Kim,[6] S. B. Kim,[14] S. H. Kim,[23] Y. K. Kim,[12] L. Kirsch,[2] K. Kondo,[23] J. Konigsberg,[8] E. Kovacs,[6] M. Krasberg,[14] S. E. Kuhlmann,[1] E. Kuns,[21] A. T. Laasanen,[18] S. Lammel,[3] J. I. Lamoureux,[25] S. Leone,[17] J. D. Lewis,[6] W. Li,[1] P. Limon,[6] M. Lindgren,[3] T. M. Liss,[9] N. Lockyer,[16] M. Loreti,[15] E. H. Low,[16] C. B. Luchini,[9] P. Lukens,[6] P. Maas,[25] K. Maeshima,[6] M. Mangano,[17] J. P. Marriner,[6] M. Mariotti,[17] R. Markeloff,[25] L. A. Markosky,[25] R. Mattingly,[2] P. McIntyre,[22] A. Menzione,[17] T. Meyer,[22] S. Mikamo,[11] M. Miller,[4] T. Mimashi,[23] S. Miscetti,[7] M. Mishina,[11] S. Miyashita,[23] Y. Morita,[23] S. Moulding,[2] J. Mueller,[21] A. Mukherjee,[6] T. Muller,[3] L. F. Nakae,[2] I. Nakano,[23] C. Nelson,[6] C. Newman-Holmes,[6] J. S. T. Ng,[8] M. Ninomiya,[23] L. Nodulman,[1] S. Ogawa,[23] R. Paoletti,[17] V. Papadimitriou,[6] A. Para,[6] E. Pare,[8] S. Park,[6] J. Patrick,[6] G. Pauletta,[17] L. Pescara,[15] T. J. Phillips,[5] F. Ptohos,[8] R. Plunkett,[6] L. Pondrom,[25] J. Proudfoot,[1] G. Punzi,[17] D. Quarrie,[6] K. Ragan,[16] G. Redlinger,[4] J. Rhoades,[25] M. Roach,[24] F. Rimondi,[6],(a) L. Ristori,[17] W. J. Robertson,[5] T. Rodrigo,[6] T. Rohaly,[16] A. Roodman,[4] W. K. Sakumoto,[19] A. Sansoni,[7] R. D. Sard,[9] A. Savoy-Navarro,[6] V. Scarpine,[9] P. Schlabach,[8] E. E. Schmidt,[6] O. Schneider,[12] M. H. Schub,[18] R. Schwitters,[8] A. Scribano,[17] S. Segler,[6] Y. Seiya,[23] M. Shapiro,[12] N. M. Shaw,[18] M. Sheaff,[25] M. Shochet,[4] J. Siegrist,[12] P. Sinervo,[16] J. Skarha,[10] K. Sliwa,[24] D. A. Smith,[17] F. D. Snider,[10] L. Song,[6] T. Song,[14] M. Spahn,[12] P. Sphicas,[13] R. St. Denis,[8] A. Stefanini,[17] G. Sullivan,[4] K. Sumorok,[13] R. L. Swartz, Jr.,[9] M. Takano,[23] K. Takikawa,[23] S. Tarem,[2] F. Tartarelli,[17] S. Tether,[13] D. Theriot,[6] M. Timko,[24] P. Tipton,[19] S. Tkaczyk,[6] A. Tollestrup,[6] J. Tonnison,[18] W. Trischuk,[8] N. Turini,[17] Y. Tsay,[4] F. Ukegawa,[23] D. Underwood,[1] S. Vejcik III,[10] R. Vidal,[6] R. G. Wagner,[1] R. L. Wagner,[6] N. Wainer,[6] J. Walsh,[16] T. Watts,[21] R. Webb,[22] C. Wendt,[25] H. Wenzel,[17] W. C. Wester III,[12] T. Westhusing,[9] S. N. White,[20] A. B. Wicklund,[1] E. Wicklund,[6] H. H. Williams,[16] B. L. Winer,[19] D. Wu,[14] J. Wyss,[15] A. Yagil,[6] K. Yasuoka,[23] G. P. Yeh,[6] J. Yoh,[6] M. Yokoyama,[23] J. C. Yun,[6] A. Zanetti,[17] F. Zetti,[17] S. Zhang,[14] and S. Zucchelli[6],(a)

(CDF Collaboration)

[1]Argonne National Laboratory, Argonne, Illinois 60439
[2]Brandeis University, Waltham, Massachusetts 02254

[3]University of California at Los Angeles, Los Angeles, California 90024
[4]University of Chicago, Chicago, Illinois 60637
[5]Duke University, Durham, North Carolina 27706
[6]Fermi National Accelerator Laboratory, Batavia, Illinois 60510
[7]Laboratori Nazionali di Frascati, Istituto Nazionale di Fisica Nucleare, Frascati, Italy
[8]Harvard University, Cambridge, Massachusetts 02138
[9]University of Illinois, Urbana, Illinois 61801
[10]The Johns Hopkins University, Baltimore, Maryland 21218
[11]National Laboratory for High Energy Physics (KEK), Ibaraki-ken, Japan
[12]Lawrence Berkeley Laboratory, Berkeley, California 94720
[13]Massachusetts Institute of Technology, Cambridge, Massachusetts 02139
[14]University of Michigan, Ann Arbor, Michigan 48109
[15]Università di Padova, Istituto Nazionale di Fisica Nucleare, Sezione di Padova, I-35131 Padova, Italy
[16]University of Pennsylvania, Philadelphia, Pennsylvania 19104
[17]Istituto Nazionale di Fisica Nucleare, University and Scuola Normale Superiore of Pisa, I-56100 Pisa, Italy
[18]Purdue University, West Lafayette, Indiana 47907
[19]University of Rochester, Rochester, New York 15627
[20]Rockefeller University, New York, New York 10021
[21]Rutgers University, Piscataway, New Jersey 08854
[22]Texas A&M University, College Station, Texas 77843
[23]University of Tsukuba, Tsukuba, Ibaraki 305, Japan
[24]Tufts University, Medford, Massachusetts 02155
[25]University of Wisconsin, Madison, Wisconsin 53706
(Received 15 June 1992)

We present a measurement of jet shapes in $\bar{p}p$ collisions at $\sqrt{s}=1.8$ TeV at the Fermilab Tevatron using the Collider Detector at Fermilab (CDF). Qualitative agreement is seen with the predictions of recent next-to-leading $[O(\alpha_s^3)]$ calculations and with leading logarithm QCD based Monte Carlo simulations. The dependence of the jet shape on transverse energy is studied.

In this Letter we report an analysis of jet shapes, measured using the momentum flow of charged particles inside jets, and the dependence of the jet shape on jet energy for jets in the 100 GeV energy range. The experimental data, gathered using the Collider Detector or Fermilab (CDF) in $\bar{p}p$ collisions at $\sqrt{s}=1.8$ TeV, are compared to the calculation of Ellis, Kunszt, and Soper [1,2] and to leading logarithm QCD Monte Carlo simulations [3,4].

Such comparisons between QCD calculations and observations in jet physics have been plagued by a lack of knowledge of the fragmentation process. Although a large amount of experimental data have been accumulated on jet fragmentation, there are still no reliable techniques to calculate QCD in this soft regime. However, the main kinematic features of the nonperturbative hadronization process can be summarized by its longitudinal and lateral properties with respect to the jet axis: The longitudinal momentum (K_l) distribution approximately scales with jet energy, apart from logarithmic violations [5-7]; the transverse momentum (K_t) spectrum of the particles in the jet has a mean K_t of ~ 350-500 MeV, which changes slowly with jet energy [5,8].

Based on the above, the mean angle δ between a particle and jet axis, where $\tan\delta = K_t/K_l$, should decrease with jet energy as K_t remains almost constant and K_l grows almost linearly with jet energy. Thus the size of a cone which contains a constant fraction of the jet energy is expected to decrease with jet energy. At high energies, however, gluon emission effects are more prominent due to scaling of the matrix elements. Therefore, at sufficiently high energies where fragmentation effects become negligible, the shape of the jet should be calculable by perturbative QCD alone.

The Fermilab Tevatron has produced the most energetic jets ever seen. Therefore, it is interesting to test whether the shape of these jets, measured by momentum flow within a cone, can indeed be calculated by an α_s^3 finite-order perturbative QCD calculation [1]. Such a calculation has been shown to agree very well with the inclusive $d^2\sigma/dE_T\,d\eta$ jet cross section [9], where $E_T = E\sin\theta$, E is the jet energy, $\eta \equiv -\ln[\tan(\theta/2)]$, and θ is the polar angle with respect to the beam. Henceforth, transverse refers to the beam (i.e., $p\bar{p}$) axis.

The CDF has been described in detail elsewhere [10]. The detector elements most relevant to this study are the central calorimeter and the central tracking chamber. The calorimeter covers the pseudorapidity range $|\eta| \leq 1.1$. This calorimeter is segmented into projective towers of $\Delta\eta \times \Delta\phi = 0.1 \times 15°$. Charged-particle momenta are measured with the central tracking chamber, a cylindrical drift chamber immersed in a 1.4 T solenoidal magnetic field parallel to the beam axis. In the pseudorapidity range $|\eta| < 1.2$, the transverse momentum resolution is $\delta P_T/P_T^2 \sim 0.002$ (GeV/c)$^{-1}$. The polar angle is measured with an accuracy $\delta\cot\theta$ of $\pm 5 \times 10^{-3}$. The detec-

tor was triggered on the presence of a localized cluster of energy in the calorimeter, comprised of a seed tower with at least 3 GeV of deposited E_T surrounded by contiguous trigger towers ($\Delta\eta \times \Delta\phi = 0.2 \times 15°$) with 1 GeV or more of deposited E_T in each [11]. In order to span a large range of cross sections, three separate thresholds of 20, 40, and 60 GeV, were imposed on the transverse energy of the trigger cluster. The 20 and 40 GeV triggers were prescaled to accept 1 in 300 and 1 in 30 events, respectively. The data set analyzed here corresponds to an integrated luminosity of 4.2 pb^{-1} at a center of mass energy $\sqrt{s} = 1.8$ TeV.

Jets are identified using a cone algorithm based on the measured event vertex as the origin. Contiguous seed towers with $E_T > 1$ GeV are selected to form preclusters. Using the E_T weighted centroid of each precluster as a starting point, jet clusters are formed by including all towers with $E_T > 0.1$ GeV inside a cone of radius $R_0 = [(\Delta\eta)^2 + (\Delta\phi)^2]^{1/2}$ (ϕ measured in radians). A tower is included in a cluster if its center is inside the cone, otherwise it is excluded. A cone of $R_0 = 1.0$ is used in this analysis to minimize the flow of energy out of the jet cone. If a cluster shares more than 75% of its energy with a cluster of higher energy, the two are merged together. Otherwise, they are defined as separate, and towers common to both clusters are assigned to the jet with the nearest centroid. Further details on this algorithm may be obtained from Ref. [11]. The jet energy, E, is determined using a scalar sum of tower energies in the cone. E_T is measured as $E\sin\theta$, where θ is the angle between a line drawn from the cluster centroid to the event vertex position and the beam line. The jet axis used in the jet shape computation is defined by the following:

$$\eta_{\text{jet}} = \frac{\sum_{\text{towers}} \eta_i E_T}{\sum_{\text{towers}} E_T}, \quad \phi_{\text{jet}} = \frac{\sum_{\text{towers}} \phi_i E_T}{\sum_{\text{towers}} E_T}. \quad (1)$$

The above algorithm is very similar to the jet definition

employed at the parton level in producing the $O(\alpha_s^3)$ predictions for comparison [1,12].

Cuts were applied on the data to ensure uniform acceptance. The event vertex was required to be within 60 cm of the center of the detector along the beam line. A minimum energy cut, based on the trigger efficiency determined with jets in the region of E_T where the data from different triggers overlapped, was applied to avoid trigger biases. A maximum energy cut was also imposed to produce three nonoverlapping samples for the study of the jet shape variation with energy. The obtained ranges were 40–60, 65–90, and 95–120 GeV, having mean energies of 45, 70, and 100 GeV for the 20, 40, and 60 GeV triggers, respectively. Background from cosmic ray showers were rejected using criteria based on timing information in the hadronic calorimeter and jet E_T balancing, similar to those described in Ref. [13]. No cuts were applied to the balancing jets. Finally, jets in the sample were required to have $0.1 \le |\eta| \le 0.7$ to ensure uniform detector response and good containment in the central detector. These cuts yielded 14725, 16793, and 60970 events for the 20, 40, and 60 GeV triggers, respectively.

Tracks were used to study the jet shapes because of their better spatial and momentum resolution for single particles. The shape distribution is obtained by histogramming for each track in a jet its distance r ($= [(\Delta\eta)^2 + (\Delta\phi)^2]^{1/2}$), weighted by its transverse momentum (P_T), and divided by the total transverse momentum carried by tracks in the jet ($\mathcal{P}_T^{\text{jet}}$). This distribution is then normalized by dividing it by the total number of jets in the sample $\mathcal{N}_{\text{jet}}$. Note that only tracks with momentum above the minimum momentum measured by the central tracking chamber P_T^{min} ($= 0.4$ GeV) and within distance $r < R_0$ ($= 1.0$) of the jet axis contribute to the distribution. N is the number of these tracks. Mathematically, the shape is defined by the normalized average transverse momentum (P_T) density $\rho(r)$:

$$\rho(r) = \frac{\xi(r)}{\int_0^{R_0} \xi(r')dr'}, \quad \text{with} \quad \xi(r) \equiv \frac{1}{\mathcal{N}_{\text{jet}}} \sum_{\text{jets}} \int_{P_T > P_T^{\text{min}}} \frac{P_T}{\mathcal{P}_T^{\text{jet}}} \frac{d^2N}{dr\,dP_T} dP_T. \quad (2)$$

The integral shape variable $\Psi(r) = \int_0^r \rho(r')dr'$ is used to compare data with theory. Note that r is related to the angle δ through the relation between η and θ: For small angles, $\Delta\eta = \Delta\theta/\sin\theta$ and $\delta = [(\Delta\theta)^2 + (\Delta\phi)^2]^{1/2}$.

The theoretical predictions for the integral jet shape are obtained by calculating the phase space for two partons, weighted by their E_T and the appropriate matrix element squared, between the inner cone r and the jet cone R_0 [2]. The result is normalized by the total Born cross section. Assuming that nonperturbative effects do not change the jet shape substantially, this quantity is $1 - \Psi(r)$, from which the theoretical $\Psi(r)$ is extracted. This procedure is used in order to avoid collinear singularities at $r = 0$. We note that the α_s^3 theory does not predict substantial differences between quark and gluon jet shapes.

In Fig. 1(a), the integrated jet shape Ψ is shown and compared with an α_s^3 calculation by Ellis for jets of 100 GeV E_T, for three different renormalization scales μ [2], and with the results of the HERWIG [3] Monte Carlo simulation, which includes fragmentation effects. Nonperturbative effects are not added to the QCD curves. It is remarkable that a pure perturbative QCD calculation can describe the experimental data so well.

The measurement of the shape $\Psi(r)$ can be distorted by various experimental effects. The dominant ones are the spatial resolution of jet axis position and tracking inefficiency at the jet core. Both effects tend to smear energy out from the core to the adjacent regions.

The tracking efficiency in jets was estimated by merging drift chamber hits from simulated tracks into real jet
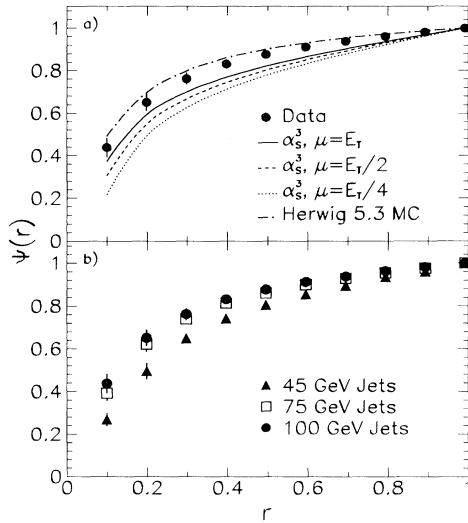
FIG. 1. (a) The distribution of the P_T fraction in a cone for 100 GeV E_T jets and cone size of $R_0 = 1.0$. The variable plotted, $\Psi(r)$, is the ratio of P_T within a cone of radius r to the P_T within a cone of radius $R_0 = 1.0$. Systematic uncertainties dominate the errors. Also shown are QCD calculations: α_s^3 theory calculations, using HMRS B structure functions for $\Lambda_{QCD} = 122$ MeV and different scales μ; the prediction from the HERWIG Monte Carlo version 5.3. (b) $\Psi(r)$ for 45, 70, and 100 GeV jets.

data, as in Ref. [6]. Those events were tracked by the same algorithm used for real data, and the resulting efficiency was parametrized as a function of the spatial separation of tracks and the jet E_T. The parametrization was incorporated in the fast detector simulation used for this analysis. The systematic uncertainty in this procedure was estimated by comparing the jet shape distribution $\Psi(r)$ obtained by generating jet events with the HERWIG Monte Carlo program, and propagating them through two different detector simulations, one which uses the efficiency parametrization, and one which generates drift chamber hits which are subsequently tracked by the CDF tracking algorithm. The difference between these two distributions was used as the systematic uncertainty. This uncertainty varies between 6% for $r < 0.1$ to less than 1% for $r > 0.4$.

The uncertainty in the jet axis position introduces a correlation in r, found to be mainly between adjacent bins in r, in the measured distribution. For example if the resolution is Δr then a particle produced at distance r from the real jet axis may be detected at $r + \Delta r$ or in a different bin. To unfold this effect, we use a correction matrix, calculated from a Monte Carlo simulation, in the following way: We determine the matrix $\mathcal{A}$, defined such that $\rho_{det} = \mathcal{A}\rho_{gen}$, where ρ_{det} is the jet shape distribution obtained from Monte Carlo detector simulation and ρ_{gen} is the generated distribution. The elements of matrix $\mathcal{A}$ are found by summing over all contributions in a bin in the space (r_{det}, r_{gen}) and the matrix is then normalized by

rows to fulfill $\rho_{det} = \mathcal{A}\rho_{gen}$. The inverse matrix $\mathcal{A}^{-1}$ is used to correct the data: $\rho_{corr} = \mathcal{A}^{-1}\rho_{meas}$, where ρ_{corr} is the corrected distribution and ρ_{meas} is the measured distribution. This procedure corrects also for known detector effects such as tracking efficiency, mentioned above. The correction is of the order of 6% for $r = 0.1$ and less than 3% for the other r bins.

The stability of the correction method was checked by the following procedure. Two correction matrices were generated with two different Monte Carlo programs, HERWIG 5.3 [3] and PYTHIA 5.4 [4]. The correction matrix of the first was applied to the obtained distribution (after detector simulation) of the second and vice versa. The result of the matrix corrections was compared with the generated distributions. The difference between the corrected and generated distributions was added to the systematic uncertainty on $\Psi(r)$. These differences vary from 7% for $r < 0.1$ to less than 1% for $r > 0.3$.

The uncertainty from the jet axis definition was estimated by comparing the jet shape distributions from Monte Carlo generated events, using two different jet axes: the jet axis obtained from the CDF jet algorithm after the events were propagated through the detector simulation, and the jet axis obtained from clustering the generated particles. The uncertainty varies from 6% at $r < 0.1$ to 1% and less for $r > 0.2$. The systematic uncertainty from fragmentation was estimated by comparing the results of the PYTHIA Monte Carlo simulation with those of the HERWIG Monte Carlo simulation. This uncertainty is less than 1% for all r.

Finally, underlying event contributions to the shape are small, as their shape is flat and the energy small compared to the jet energies used. The calorimeter energy scale is uncertain to 3% and this leads to a systematic uncertainty in the jet shape measurement which varies from 4% for $r < 0.1$ to less than 1% for $r > 0.2$.

The total systematic uncertainty was estimated by adding all above sources in quadrature. For $r < 0.1$, the uncertainty ranges from 12% of $\Psi(r)$ for the lowest jet energy studied, to 10% for the highest. For $r > 0.5$ the uncertainty is less than 1% for the three jet energies.

A 100 GeV E_T jet has, on average, 50% of its transverse momentum carried by approximately fourteen measured tracks within a cone of 1.0. As an additional check, we compared the jet shape distribution obtained from tracks to the one obtained from calorimeter information. No significant differences were found.

In Fig. 1(b), Ψ is plotted for the three different energies, 45, 70, and 100 GeV. One can observe that the jets get narrower as their E_T increases. In order to compare the data to theory and to QCD Monte Carlo simulations, the energy dependence of the shape is shown in Fig. 2 by plotting the fractional P_T inside of a cone of $r = 0.4$, for the three different energies. Also plotted are the predictions of the HERWIG and PYTHIA Monte Carlo simulations, with their respective default structure functions, DO [14] and EHLQ [15], and the predictions of the α_s^3
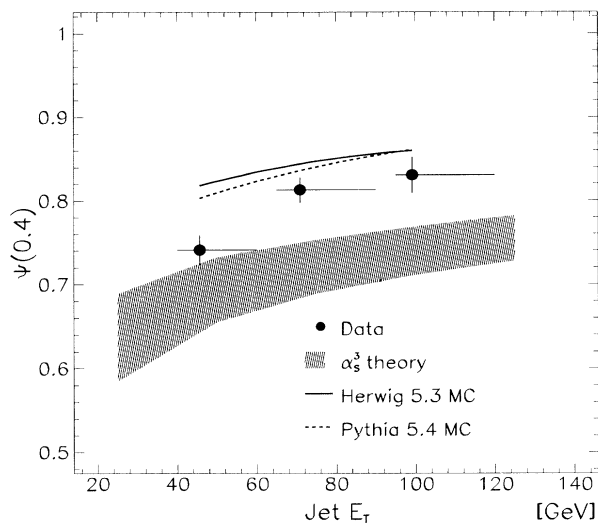
FIG. 2. $\Psi(0.4)$ for 45, 70, and 100 GeV jets. The horizontal error bars represent the jet E_T range. Systematic uncertainties dominate the vertical error bars. Also shown are predictions from the α_s^3 theory (the width of the band representing the μ dependence), and from the HERWIG and PYTHIA Monte Carlo simulations.

theory, using HMRS B [16]. The bands represent the uncertainty in the α_s^3 theory due to the renormalization scale.

Both the α_s^3 theory and the leading logarithm shower Monte Carlo simulations agree qualitatively with the data, although it seems that the jets are slightly more collimated than the α_s^3 theory and slightly less collimated than the prediction of the shower Monte Carlo simulations. One possible explanation for the observation that high-energy jets are narrower than the α_s^3 prediction is that higher-order effects tend, through coherent gluon emission [17], to populate with soft partons the region between the "hard" emission and the original parton, transferring some of the energy of the hard parton to the inner part of the jet. As a result of the details of jet merging in our jet finding algorithm, one cannot directly compare this measurement to our previous measurement of the variation of the inclusive jet cross section with cone size [9].

In conclusion, it is encouraging that the calculation of the jet internal structure by a perturbative expansion in α_s is so close to the experimental data. This might be the first step in understanding jet formation from first princi-

ples, without relying on phenomenological models.

(a)Visitor.

[1] S. D. Ellis, Z. Kunszt, and D. E. Soper, Phys. Rev. Lett. **64**, 2121 (1990).

[2] S. D. Ellis, Z. Kunszt, and D. E. Soper, in Proceedings of the Lepton-Hadron Conference, Geneva, 1991 [Report No. UW/PT-91-13 (to be published)]; Report No. UW/PT-92-01 (to be published); S. D. Ellis (private communication).

[3] G. Marchesini and B. R. Webber, Nucl. Phys. **B310**, 461 (1988).

[4] H. U. Bengtsson and T. Sjostrand, Comput. Phys. Commun. **46**, 43 (1987); T. Sjostrand, Comput. Phys. Commun. **39**, 347 (1986).

[5] TASSO Collaboration, M. Althoff *et al.*, Z. Phys. C **22**, 307 (1984).

[6] CDF Collaboration, F. Abe *et al.*, Phys. Rev. Lett. **65**, 968 (1990).

[7] Mark II Collaboration, G. S. Abrams *et al.*, Phys. Rev. Lett. **64**, 1334 (1990).

[8] Amy Collaboration, Y. K. Li *et al.*, Phys. Rev. D **41**, 2675 (1990).

[9] CDF Collaboration, F. Abe *et al.*, Phys. Rev. Lett. **68**, 1104 (1992).

[10] CDF Collaboration, F. Abe *et al.*, Nucl. Instrum. Methods, Phys. Res., Sect. A **271**, 387 (1988).

[11] CDF Collaboration, F. Abe *et al.*, Phys. Rev. D **45**, 1448 (1992).

[12] J. E. Huth *et al.*, Report No. FERMILAB-CONF-90-249-E, Snowmass, 1990 (to be published).

[13] CDF Collaboration, F. Abe *et al.*, Phys. Rev. Lett. **62**, 613 (1989).

[14] D. W. Duke and J. F. Owens, Phys. Rev. D **30**, 49 (1984).

[15] E. Eichten, I. Kinchliffe, K. Lane, and C. Quigg, Rev. Mod. Phys. **56**, 579 (1984).

[16] P. Harriman, A. Martin, R. Roberts, and W. Stirling, Phys. Rev. D **42**, 798 (1990).

[17] A. Bassetto, M. Ciafaloni, and G. Marchesini, Phys. Rep. **100**, 202 (1983).